JACS
JOURNAL OF THE AMERICAN CHEMICAL SOCIETY
pubs.acs.org/JACS
Article

The Competition between Hydrogen, Halogen, and Covalent Bonding in Atmospherically Relevant Ammonium Iodate Clusters

Nicoline C. Frederiks, Danika D. Heaney, John J. Kreinbihl, and Christopher J. Johnson*

Cite This: J. Am. Chem. Soc. 2023, 145, 1165−1175
Read Online
ACCESS | Metrics & More | Article Recommendations | Supporting Information

ABSTRACT: Iodine-containing clusters are expected to be central to new particle formation (NPF) events in polar and midlatitude coastal regions. Iodine oxoacids and iodine oxides are observed in newly formed clusters, and in more polluted midlatitude settings, theoretical studies suggest ammonia may increase growth rates. Structural information was obtained via infrared (IR) spectroscopy and quantum chemical calculations for a series of clusters containing ammonia, iodic acid, and iodine pentoxide. Structures for five of the smallest cationic clusters present in the mass spectrum were identified, and four of the structures were found to preferentially form halogen and/or covalent bonds over hydrogen bonds. Ammonia is important in proton transfer from iodic acid components and also provides a scaffold to template the formation of a halogen and covalent bonded backbone. The calculations executed for the two largest clusters studied suggested the formation of a covalent $I_3O_8^-$ anion within the clusters.

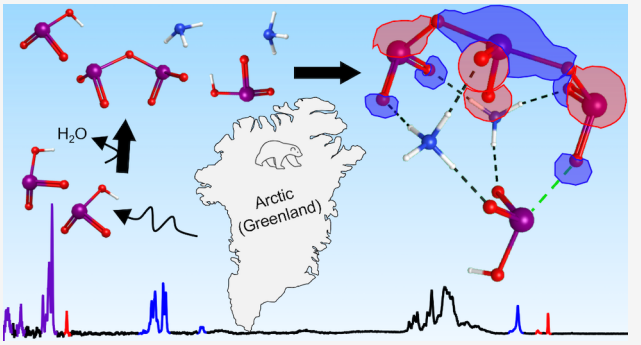

INTRODUCTION

New particle formation (NPF) is responsible for the birth of approximately 50% of aerosol particles formed in the atmosphere,[1] and results from the clustering of low volatility gaseous vapors.[2] Acid−base chemistry and salt bridge formation play an important role in stabilizing early stage NPF clusters against evaporation, allowing these clusters to grow into atmospherically relevant sizes.[3−9] Sulfuric acid−ammonia (−water) clusters have previously been studied in depth[10−15] as these particles make up a majority of postindustrial revolution NPF contributors.[16] However, in midlatitude coastal and polar regional NPF events, H_2SO_4−NH_3(−H_2O) cluster formation rates alone could not account for observed NPF rates.[17,18] Further investigation into these regional events led to the discovery that the presence of iodine in these regions helps fuel these NPF events.[19−22] Coastal algae and other biota release I_2,[23−26] HOI,[27,28] and various organo-iodide species, such as CH_2I_2,[20,21,29−31] at low tide, which can form various iodine oxoacids[23,32−36] and iodine oxides[19,22,31,32,37−42] through photolysis and photooxidation. Coastal nutrient enhancement, likely due to runoff, has greatly increased the algae population along with other anthropogenic emissions on and near the coast of China and has resulted in regionally high iodine concentrations.[43] Since preindustrial times, it is believed that there has been a 70% increase in atmospheric iodine.[44] I^- in seawater in the presence of ample ozone concentrations, can also lead to the formation and emission of various organo-iodide compounds into the atmosphere.[45−47] During the day, if concentrations of CH_2I_2 are in the 10s of ppt range, NPF can take place without any other contributing species.[30] It has even been found that iodine oxoacid nucleation rates are higher than those of sulfuric acid−ammonia clusters at equal concentrations of acids.[48] In the Arctic, over pack ice, chemical ionization mass spectrometry measurements suggest that the concentration of iodic acid is 6−10 times higher than that of sulfuric acid, and as a result NPF events are primarily centered around HIO_3, with minimal participation from sulfuric acid and other species.[33] However, the role of gas phase HIO_3 is unclear as some fraction of the detected iodic acid may result from the chemical ionization process.[49]

Since acid−base chemistry plays such an important role in these early stage NPF clusters, the role of ammonia has also been explored in iodine containing clusters as it is important in stabilizing sulfuric acid and nitric acid containing clusters.[50,51] Quantum chemical calculations found that ammonia can aid in the hydrolysis of I_2O_5 and it can also interact with HIO_3, increasing nucleation rates of these clusters through the lowering of transition state energies via increased hydrogen

Received: October 12, 2022
Published: January 3, 2023

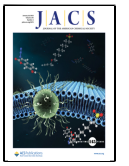

https://doi.org/10.1021/jacs.2c10841
J. Am. Chem. Soc. 2023, 145, 1165−1175

bond donors and acid−base interactions.[50] Further calculations and atmospheric cluster dynamics code (ACDC) simulations probing the role of sulfuric acid and ammonia on iodic acid nucleation rates also found that ammonia can help stabilize these clusters and enhance growth rates.[51] However, we are aware of no direct experimental evidence for the compositions or structures of such clusters.

There has been some debate on whether or not iodine oxides, such as I_2O_{3-5}, are the driving force behind the formation of these clusters or whether HIO_3 and iodine oxoacids play a more substantial role. In solution, it has been shown that iodic acid dimers can directly form I_2O_5 via a single dehydration reaction even though it has typically been believed to be a multiple step process.[52] Nevertheless, quantum chemical exploration of the dehydration of iodic acid into iodine pentoxide has been found to be kinetically unfavorable in the gas phase due to the presence of significant transition state barriers.[53,54] In the Arctic Ocean, it has been suggested that iodic acid propels NPF events,[33] and other studies have also identified high concentrations of atmospheric iodic acid and concluded that clustering of HIO_3 is the dominant formation pathway, with the formation of I_2O_5 resulting from internal cluster rearrangement.[34] However, uncertainty in the role of the chemical ionization process may require revisiting these results. Studies of the hydrolysis of iodine oxides and atomic iodine to form HIO_3 determined that water reacts slowly with these components and that gas phase iodic acid is not imperative for the presence of HIO_3 in these particles, suggesting that clustering of iodine oxides is the primary channel of this type of cluster formation.[36] Yet, specific relative humidity ranges of less than 65% have been found to promote this hydrolysis reaction of I_2O_5 to HIO_3, which is an atmospherically plausible range.[55] A more recent chemical ionization mass spectrometric study concluded that, in dry environments, iodine oxides are likely the driving force behind NPF, whereas in more humid environments both iodine oxides and HIO_3 contribute to NPF.[49] The importance of iodine oxides beyond cluster conception has been a source of controversy as well. IO_2, for example, has been suggested to play a more crucial role in the early growth stages compared to initial cluster formation.[56] Taken together, these observations paint a complex picture of the chemical transformations experienced by iodine-rich new particles.

Despite the field studies,[18,29,31,33,34,41−43,57,58] quantum chemical simulations,[44,50,51,53,54,56,59,60] and laboratory experiments[19,30,32,48,61−64] focusing on iodine-containing atmospheric new particles, there has been relatively little experimental work probing the structures of these clusters.[55] Here, we use infrared spectroscopy of mass-selected clusters to explore the structural motifs present in stable clusters of up to five total molecules to show that even these small clusters feature a complex array of bonding interactions likely driving their growth, highlighting the potential role of even larger iodine oxides previously isolated in inorganic crystals in stabilization of clusters.

EXPERIMENTAL SECTION

The clusters discussed in this work were formed by spraying a 5 mM iodic acid/10 mM ammonium hydroxide solution in a 50/50 water/methanol solution with 0.1% formic acid on an electrospray ionization (ESI) source. These clusters were generated on two different instruments: a Thermo Scientific LTQ XL linear trap mass spectrometer and a home-built guided ion beam/ion trap/tandem time-of-flight (TOF) photofragmentation mass spectrometer discussed in detail in previous work.[65] The mass spectrum displayed in Figure 1 was recorded on the LTQ XL, which provided insight into

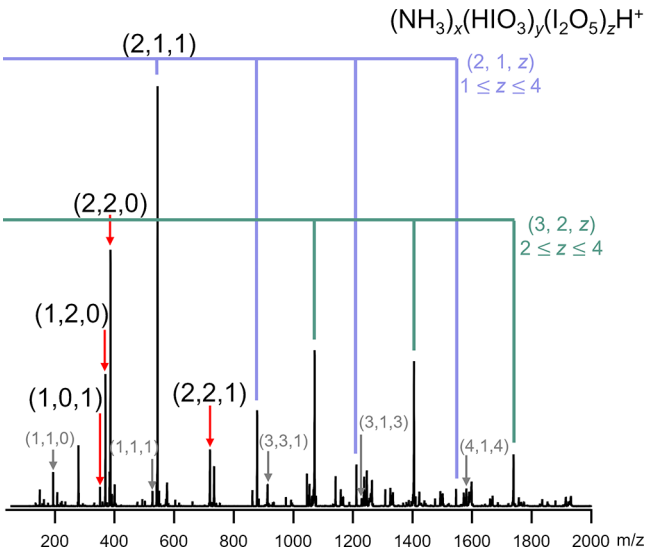

Figure 1. Mass spectrum of 5 mM iodic acid/10 mM ammonium hydroxide solution in 50/50 water/methanol with 0.1% formic acid. The (2, 1, z) cluster series is shown in purple and the (3, 2, z) cluster series is shown in green. Other identified clusters are shown in gray. The clusters discussed in depth in this paper are listed in black, with red arrows.

the cluster compositions derived from this mixture. Further analysis took place through mass spectrometry coupled to infrared (IR) spectroscopy carried out on the home-built guided ion beam/ion trap/tandem time-of-flight (TOF) photofragmentation mass spectrometer.

Briefly, the ions are formed in an atmospherically isolated ESI source, where they are then guided through a series of ion guides to a cryogenically cooled octopole ion trap. Inside the cryogenically cooled trap (cooled by Sumitomo RDK-408D2 cold head), the ions are collisionally cooled via introduction of pulsed helium gas. Most spectra of the clusters discussed herein were recorded via cryogenic ion vibrational predissociation (CIVP),[66] where an inert tag species, in this case N_2 gas, is seeded into the cryogenic ion trap. The trap is cooled down to approximately 45 K in order for the tag to physisorb onto the cluster of interest. The tagged ion packet is then accelerated down a field free flight tube to the laser crossing, where a portion of the ion packet is intersected by tunable infrared laser light produced by a Nd:YAG-pumped OPO/OPA system (LaserVision). As the laser scans, the tagged cluster will absorb a single photon when resonant with an IR transition, resulting in the tag desorbing from the cluster. A reflectron then separates the ions that lose a tag from those that did not, before they reach the microchannel plate detector. Spectra are computed from the ratio of untagged ions to tagged plus untagged ions multiplied by laser power, as a function of wavelength. CIVP allows for the collection of a linear spectrum, and therefore direct comparisons of relative peak intensities can be made.

All of the calculations discussed in this work were performed using the Gaussian 16 suite of programs.[67] The density functional CAM-B3LYP was used with a split basis set of aug-cc-pVDZ on light atoms and Def2-SV(P) on iodine. The rationale for this choice is discussed in the Supporting Information. Spectra from harmonic frequency calculations are presented without scaling.[68] All relative energies include zero-point energy.

RESULTS AND DISCUSSION

1. Observation of Stable Clusters by Mass Spectrometry. Figure 1 displays a mass spectrum featuring a series of

https://doi.org/10.1021/jacs.2c10841
J. Am. Chem. Soc. 2023, 145, 1165−1175

singly protonated cationic clusters containing various numbers of ammonia, iodic acid, and iodine pentoxide molecules. The clusters discussed in this paper will be referred to using the following nomenclature assignment: $(x, y, z) = (NH_3)_x(HIO_3)_y(I_2O_5)_zH^+$. There are several patterns that seem to appear as the clusters begin to grow larger in size. One of which involves the $(3, 2, z)$ clusters, where $2 \leq z \leq 4$. Above 1000 m/z these are the most prominent peaks in the mass spectrum suggesting that these clusters form most readily and are relatively stable. This group of clusters grows via the addition of a single I_2O_5 and has a consistent number of three ammonia and two iodic acid molecules. Their growth mechanism, by iodine pentoxide with an unchanging number of ammonia and iodic acid molecules, could suggest that once a cluster has sufficient ammonia and iodic acid molecules, the growth of these clusters is driven predominantly by the addition of iodine pentoxide to larger, more atmospherically relevant sizes.

A similar cluster trend can be observed with the $(2, 1, z)$ clusters, where $1 \leq z \leq 4$. These clusters follow the same growth pattern as the $(3, 2, z)$ clusters discussed above, where the addition of an iodine pentoxide appears to be the main growth channel. Beyond the $(2, 1, 1)$ cluster, the peak intensities of the $(2, 1, z)$ cluster series are considerably lower than those of the $(3, 2, z)$ cluster series, and also decrease in intensity at a much faster rate with each additional iodine pentoxide, suggesting lower stability of the $(2, 1, z)$ clusters. The $(3, 2, z)$ series clusters appear to be able to accommodate more iodine pentoxide molecules, likely due to the larger number of potential stabilizing hydrogen bonds and salt bridge formation. These trends suggest that ammonia in these clusters may be important to supporting further growth via iodine pentoxide. We will focus on the $(1, 0, 1)$, $(1, 2, 0)$, $(2, 2, 0)$, $(2, 1, 1)$, and $(2, 2, 1)$ clusters, which appear to be relatively stable and serve as a starting point for analysis of larger clusters.

2. The (1, 0, 1) Cluster. The smallest cluster examined via IR spectroscopy was the $(1, 0, 1)$ cluster. This cluster contains only one ammonia and one iodine pentoxide molecule. Figure 2 displays the experimental spectrum (top) compared to the two calculated spectra for this cluster (bottom). The main features of the experimental spectrum include free NH_2 symmetric and asymmetric stretching modes around 3300−3400 cm^{-1}, the NH_2 twisting mode around 1650 cm^{-1}, NH_2 bending and wagging modes around 1400 cm^{-1}, and the IO stretching modes below 1000 cm^{-1}. There is also a large, broad hydrogen bonded NH stretching anharmonic feature spanning 2700−3250 cm^{-1}, which is typically ignored since harmonic calculations cannot accurately reproduce this region.[69−72] We performed calculations and then compared these computed spectra to the experimentally collected spectrum in order to identify key spectral features that could then ideally be tracked in larger clusters. Both calculations performed on the $(1, 0, 1)$ cluster and displayed in Figure 2 are very close in energy to each other, essentially isoenergetic, and their energy difference is within the error of the calculation. From an energetic standpoint, its possible that both of these isomers exist in experiment. Neither individual calculation appears to capture the experimental spectrum exactly, most notably in the free NH_2 stretching region, as well as in the NH_2 bending/wagging region. In the experimental spectrum there is splitting in the free NH_2 symmetric stretching region that suggests the presence of isomers, whether they be structural isomers or tag isomers. In Figure S2, both untagged calculations along

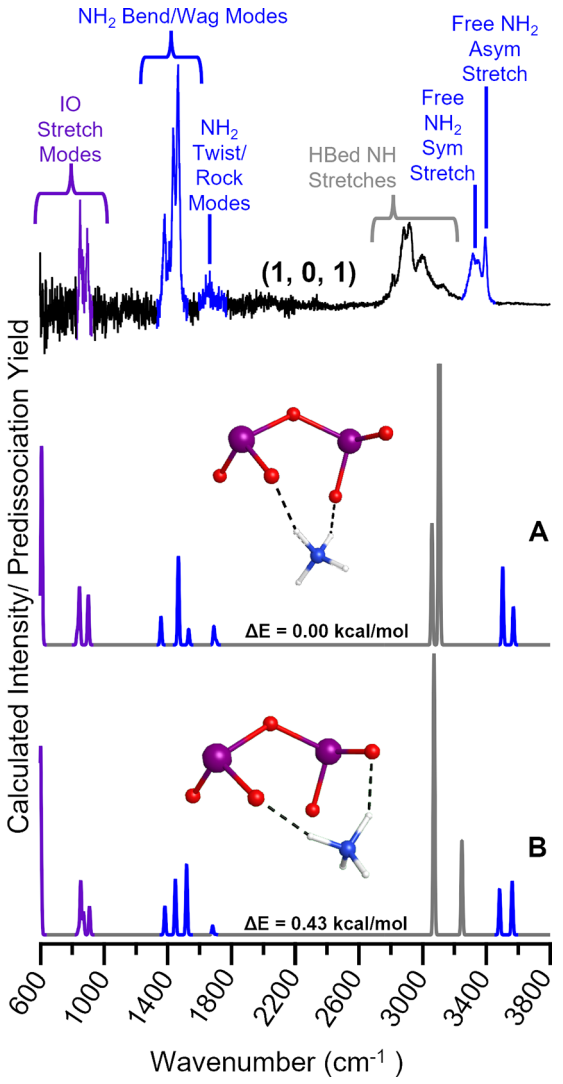

Figure 2. Experimental CIVP spectrum (top) is compared to the computed harmonic IR spectra (bottom) of the $(1, 0, 1)$ cluster. Isomer A is lowest in energy, followed by isomer B. The main features involve NH stretching and bending modes (peaks shown in blue) along with the IO stretching modes (peaks shown in purple). Neither spectrum individually convincingly captures the features present in the experimental spectrum.

with all possible tag location calculations are compared to the experimental $(1, 0, 1)$ spectrum. The tag calculations appear to drastically enhance the relative free NH stretching intensities, whereas in the experimental spectrum, there is not an evident intensity enhancement in this region. Although it is possible that tag effects could emphasize differences between the calculated and experimental spectra, it is likely not the only source of the spectral discrepancies in this case, as none of the NH_2 mode relative intensity patterns are captured any more closely in the tagged calculated spectra (Figure S2).[73] However, if we observe Figure S3 in the Supporting Information, with the overlay of the two (untagged) calculated spectra, it shows that it is highly likely that both isomers exist experimentally, as the overlaid spectra more closely capture the spectral features in the free NH_2 stretching region and the relative intensity pattern of the NH_2 bending/wagging modes in the fingerprint region are more appropriately reproduced.

https://doi.org/10.1021/jacs.2c10841
J. Am. Chem. Soc. 2023, 145, 1165−1175

Unfortunately, as we can see even at the smallest cluster size explored, iodine-local stretches and bends are not particularly diagnostic in identifying likely structure using IR spectroscopy. This is likely due to a couple of factors. One is that the iodine containing modes take place at the lower end of the region of wavenumbers that we are able to scan. The power from the laser begins to drop off significantly below 1000 cm^{-1}, reducing signal-to-noise, making it difficult to clearly see all features in this region. Second, the binding energy of N_2 is around 800 cm^{-1}, so peaks below and around this cutoff will not necessarily be well represented within the experimental spectrum. Therefore, for the (1, 0, 1) cluster and the other clusters discussed in the upcoming sections, the ammonium and OH related modes are the most reliable for determining the structure of the clusters.

3. The (1, 2, 0) Cluster. Moving on to the larger (1, 2, 0) cluster in Figure 3, we begin to see more vibrational modes appear, most notably above 3400 cm^{-1}. Since this cluster contains two iodic acid molecules and is singly protonated, we expect both iodic acid molecules to remain protonated resulting in the presence of OH modes in the experimental spectrum. We do see both free OH stretching and NH_2 asymmetric and symmetric stretching modes implying that the experimentally present isomer contains at least one free iodic acid OH as well as two non-hydrogen bonded NHs. We also see what looks to be two peaks between 1000 and 1200 cm^{-1}, which are below the typical NH bending and wagging mode region and generally indicative of either a free or hydrogen bonded OH bending mode. The hydrogen bonded OH bend in the previously studied $(NH_3)_4(H_2SO_4)_3H^+$ dry and hydrated clusters was found to lie between 1300 and 1400 cm^{-1},[14,15] which would imply that the higher energy mode closer to 1200 cm^{-1} is presumably a hydrogen bonded OH bending mode and the lower energy, lower intensity peak is possibly a free OH bend. These features allow us to eliminate the likelihood of the presence of isomer B in the experimental spectrum. The experimentally present structure is therefore likely isomer A, where there are both a free NH_2 and OH component, as well as a hydrogen bonded OH component. The relative intensity pattern within the fingerprint region of the experimental spectrum is also strikingly similar to that of isomer A, with the IO stretching modes around 800 cm^{-1} most closely reproduced in the calculated spectrum of isomer A too.

None of the calculations were able to properly replicate the splitting of the higher energy peaks associated with the free NH and OH stretching modes above 3300 cm^{-1} in the experimental spectrum. As mentioned in the (1, 0, 1) discussion, this splitting usually implies the existence of experimental isomers. However, since isomer B can be eliminated due to its lack of a free OH stretching peak, we turn to the calculations including N_2 tags performed on isomer A in Figure S4 to further interpret this splitting. There are three possible tag locations in this arrangement, and these include the free OH or one of the two free NHs. Upon comparison, these three tagged isomer spectra hint at the presence of isomers based on tag location, and not structural isomers, and all three fall within a roughly 0.2 kcal/mol range. The free symmetric NH_2, free asymmetric NH_2, and free OH stretches exhibit splitting, and the presence of a very small red-shifted free OH stretching peak suggests that all three tag isomers exist in experiment.

Previous work on ammonium bisulfate clusters found that hydrogen bonding and salt bridge formation were crucial

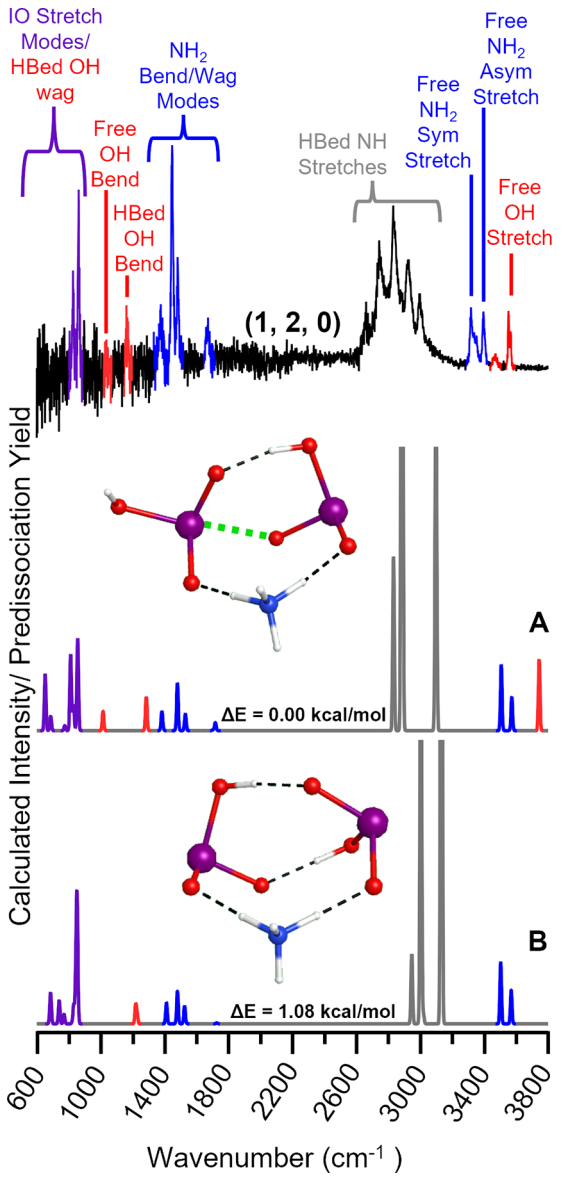

Figure 3. Experimental CIVP spectrum (top) is compared to the computed harmonic IR spectra (bottom) of the (1, 2, 0) cluster. The main features involve free OH stretching and bending modes (peaks in red), NH stretching and bending modes (peaks in blue), and IO stretching modes (peaks in purple). Isomer A is found to be the best match to the experimental spectrum, as it contains both free OH and NH stretches and the fingerprint relative peak intensity pattern is well reproduced. Therefore, isomer A is believed to be the experimentally present structure. The green dashed line in the isomer A structure represents a halogen bonding interaction.

interaction forces at play in stabilizing these clusters against evaporation and for further growth into larger sizes.[10−15] However, comparing isomer B to the experimentally present isomer A exemplifies that, for iodic acid containing clusters, halogen bonding may outcompete hydrogen bonding. Isomer B has four hydrogen bonds, whereas isomer A features only three, but also contains an apparent halogen bonding interaction (shown as a green dashed line in Figure 3). Both halogen and hydrogen bonding have previously been found to be important in iodic acid−methanesulfonic clusters explored via ACDC.[59] Yet, this finding for the (1, 2, 0) cluster suggests

https://doi.org/10.1021/jacs.2c10841
J. Am. Chem. Soc. 2023, 145, 1165−1175

that halogen bonding may be more important than hydrogen bonding in terms of stabilizing this cluster.

4. The (2, 2, 0) Cluster. The next largest cluster explored was the (2, 2, 0) cluster. Figure 4 shows the experimental and calculated structures of the (2, 2, 0) cluster. In the experimental spectrum we see the presence of a free OH stretch and both free symmetric and asymmetric NH_2 stretches, suggesting at least one iodic acid molecule remains protonated. Again the fingerprint region is dominated by the NH_2 bending/wagging modes with the iodine related stretches showing up below 1000 cm^{-1}.

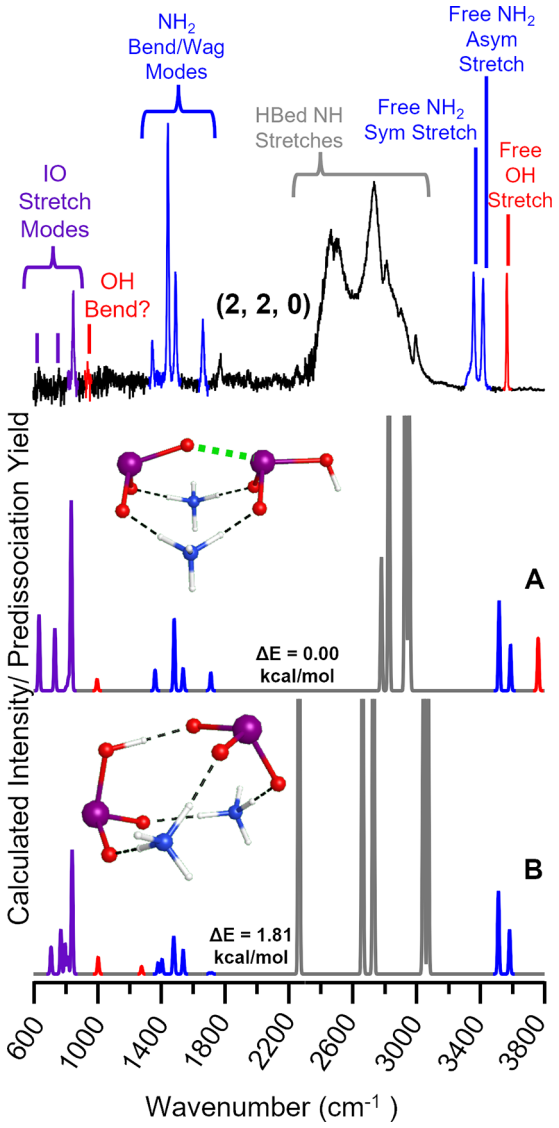

Figure 4. Experimental CIVP spectrum (top) is compared to the computed harmonic IR spectra (bottom) of the (2, 2, 0) cluster. Isomer A is lowest in energy, followed by isomer B. The main features involve OH stretching and bending modes (peaks in red), NH stretching and bending modes (peaks in blue), and IO stretching modes (peaks in purple). Again, the lowest energy isomer, A, is found to be the likely experimentally present isomer as it has a free OH stretching mode and two free NH stretching modes. The fingerprint relative peak intensity pattern composed of NH bending and wagging modes, an OH bend, and IO stretching modes is also very well replicated. The green dashed line in the isomer A structure represents a halogen bonding interaction.

Isomer B is much closer in energy to the lowest energy isomer A, but isomer B does not have a free OH. Although it was mentioned previously that the iodine related vibrational modes pose challenges in being diagnostic of structure, they can still help dismiss unlikely structures. For this cluster, in the experimental spectrum we see a sharp well-defined IO related stretching mode just above 800 cm^{-1}, and the presence of two very faint peaks, one just below 800 cm^{-1} and one just above 600 cm^{-1} (both denoted by purple lines in the experimental spectrum in Figure 4). The low intensity of these peaks is likely due to the N_2 binding energy of about 800 cm^{-1} as mentioned earlier. These iodine-related peaks are best reproduced in the lowest energy calculated spectrum of isomer A, along with the NH_2 bending/wagging modes and free NH_2 and OH stretching modes. The similarities between the calculated spectrum of isomer A and the experimental spectrum and the determination of isomer A as the lowest energy isomer suggest that isomer A is the experimentally present structure at the (2, 2, 0) cluster size.

As with the (1, 2, 0) cluster, we find that in the (2, 2, 0) cluster our experimentally present structure has the fewest hydrogen bonds of all the structures explored. Isomer B has five hydrogen bonds, whereas isomer A only has four. Again we find a minimum energy structure featuring a halogen bond. The non-hydrogen bonded oxygen on the iodate molecule appears to form a halogen bonding interaction with the iodine of the iodic acid molecule, resulting in what could be called a halogen bonded backbone of the cluster (shown as a dotted green line in Figure 4). In both cases where we have seen halogen bonding there have only been ammonia and iodic acid molecules; will this trend persist if an iodine pentoxide molecule is added to the cluster?

5. The (2, 1, 1) Cluster. Figure 5 displays the CIVP spectrum of the smallest cluster studied that is comprised of at least one ammonia, one iodic acid, and one iodine pentoxide, the (2, 1, 1) cluster. Figure 5 also shows the computed spectra for the three calculations found to be lowest in energy. Looking at the experimental spectrum, we can immediately see that there are no free OH stretches and likely no OH bends, suggesting a full proton transfer has taken place from the iodic acid to an ammonia. The vibrational modes that dominate this spectrum are free NH_2 symmetric and asymmetric stretching modes around 3400 cm^{-1}, NH_2 and NH_3 bending and wagging modes around 1400 and 1600 cm^{-1}, and the IO stretching modes around 600 and 800 cm^{-1}. The fact that the NH_2 symmetric and asymmetric stretching modes are intact at this cluster size suggests that the experimentally present structure is highly symmetric.

The lowest energy calculations displayed in Figure 5, isomers A and B, exhibit similar binding arrangements to each other with slight modifications. Isomer B exhibits full proton transfer from the iodic acid to ammonia, such that the cluster is comprised of two ammoniums, one iodate, and an iodine pentoxide molecule. Isomer A contains the same proton transfer components as isomer B, and structurally they both only differ by the orientation and subsequent hydrogen bonds of a terminal IO_3. Although visually isomer A and B do not appear to differ significantly, their predicted spectra show considerable differences in both fingerprint and NH/NH_2 stretching regions. Comparing them both directly to the experimental spectrum, we see that isomer A is an excellent match to the experimental spectrum. Isomer A has two transitions in the free NH/NH_2 stretching region, as does the

https://doi.org/10.1021/jacs.2c10841
J. Am. Chem. Soc. 2023, 145, 1165−1175

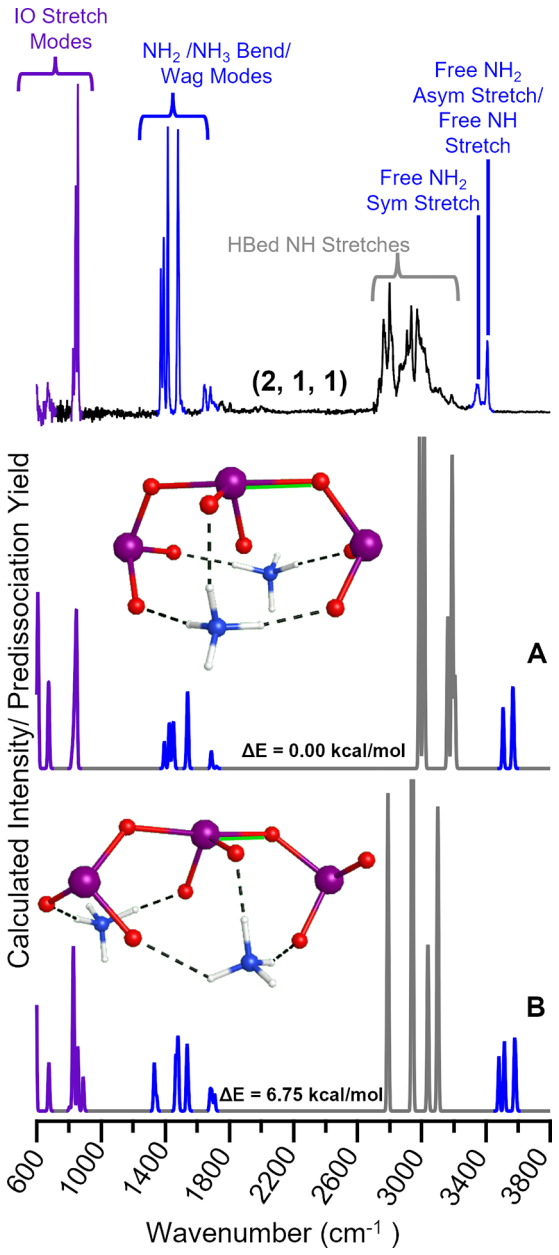

Figure 5. Experimental CIVP spectrum (top) is compared to the computed harmonic IR spectra (bottom) of the (2, 1, 1) cluster. Isomer A is lowest in energy, followed by isomer B. The main features involve NH stretching and bending modes (peaks in blue) and IO stretching modes (peaks in purple). Isomer A is found to be the experimentally present isomer as it reproduces the relative peak intensity pattern of the NH modes particularly well in both the fingerprint region and higher energy stretching region. Isomer A is also the lowest energy isomer. The solid green line underlining the covalent bond in both structures represents likely intracluster covalent bond formation.

experiment, whereas isomer B has three transitions there. Moving down to the fingerprint region, we find the relative intensity pattern of isomer A to be more representative to that of the experiment. In this region in isomer B, the relative intensity pattern is not well reproduced as there are a couple transitions (somewhat overlapped) just above 1300 cm^{-1} that do not exist in the experimental spectrum. Although the transitions in the IO stretching region just above 800 cm^{-1} in the isomer A spectrum are not as well resolved as they are in the experiment, the ascending relative intensity pattern is present with ascending wavenumber unlike in the predicted spectrum of isomer B. Taken together, isomer A is assigned as the experimentally present structure for the (2, 1, 1) cluster.

The two lowest energy calculations (in Figure 5) exhibit the same number of hydrogen bonds between the cluster constituents, unlike the higher energy calculations of the smaller halogen bonded clusters previously discussed. Another dissimilarity between the (2, 1, 1) cluster and the smaller clusters of this class emerges, where we see what appears to be equal bond lengths between the central iodine and two neighboring oxygens, as well as identical bond lengths of the central oxygens to the outer iodine molecules in isomer A. These bond lengths are shorter than the previously explored halogen bond lengths and therefore suggest that a stronger interaction than a halogen bond might be forming. However, we will discuss this interaction in more detail in the upcoming sections. Irrespective of the classification of this interaction, it results in the continuation of the O−I−O backbone, and emphasizes the importance of the ammonium hydrogen-bonded scaffold in facilitating an optimal orientation of I_2O_5 and IO_3^- for an interaction to take place.

6. The (2, 2, 1) Cluster. The final and largest cluster to be discussed is the (2, 2, 1) cluster. Figure 6 displays the three lowest energy calculated spectra compared to the experimental spectrum. Figure S11 in the Supporting Information contains all of the structures and calculated spectra explored at this cluster size. The experimental spectrum contains a single free OH stretch, and now only contains a single free NH stretch unlike the smaller clusters of this class. The single, somewhat broad NH stretch suggests that both ammoniums are likely triply hydrogen bonded and mostly symmetric. There is a broad tail on the lower wavenumber side of this peak, which is presumably due to tag effects, as that bump does not appear in the infrared multiphoton dissociation (IRMPD) spectrum in the SI (Figure S10). There is also a very small free OH stretch peak (highlighted in red) in the experimental spectrum red-shifted from the more prominent, labeled free OH stretch that is also likely the result of tag isomers (tag on OH versus tag on NH). The IRMPD spectrum of this cluster does not contain this peak, further supporting this claim.

Unlike in the (2, 1, 1) cluster case, all three lowest energy isomers (A, B, and C) are quite similar in energy. However, the experimental spectrum has several key features that allow the assignment of the experimentally present isomer to be relatively straightforward. One feature is the presence of the free OH stretch in the experimental spectrum. Another feature is the two sets of doublets between 1400 and 1500 cm^{-1} in the NH_2/ NH_3 bending/wagging mode region. The final feature is the presence of a free OH bend. Using these three vibrational mode regions, both isomers B and C can be eliminated almost immediately. Only isomer A has a free OH and can therefore be the only structure to have both free OH stretch and bend present in the predicted spectrum. Isomer A is also the only structure whose predicted spectrum has two sets of doublets in the NH_2/NH_3 bending/wagging mode region. The spectrum of isomer A appropriately reproduces the free NH stretch, NH_2 twist mode, and the majority of the relative intensity pattern of the IO stretching modes above 700 cm^{-1}. As a result isomer A once again was found to be the experimentally present structure.

Halogen bonding once again plays a crucial role in this cluster; however, only isomer A contains a halogen bond along

https://doi.org/10.1021/jacs.2c10841
J. Am. Chem. Soc. 2023, 145, 1165−1175

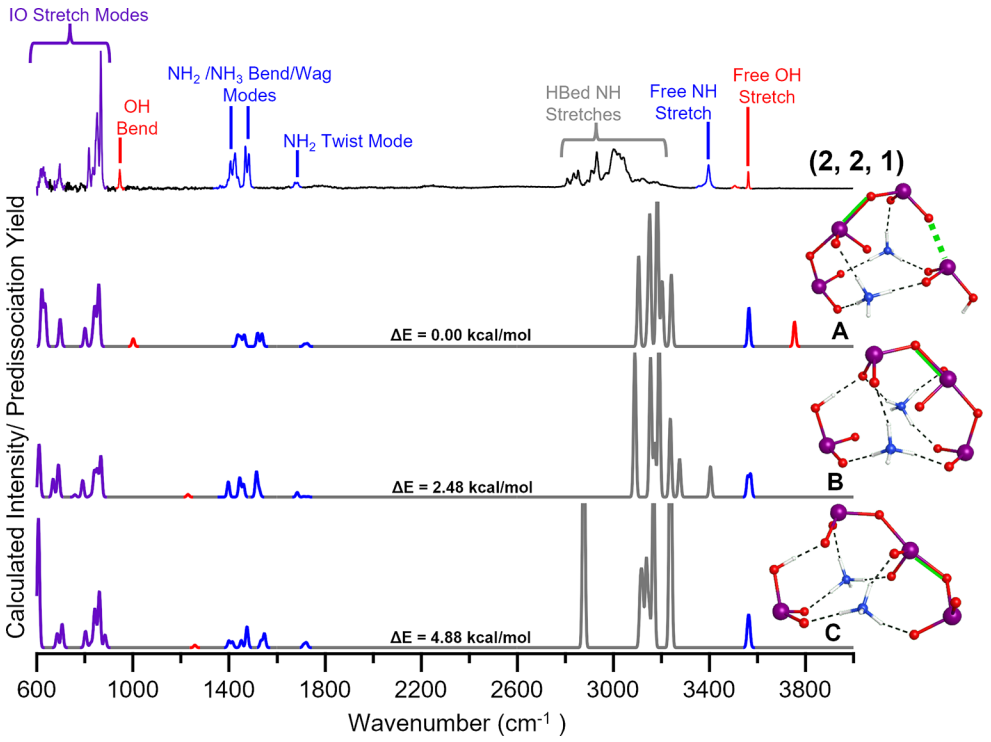

Figure 6. Experimental CIVP spectrum (top) is compared to the computed harmonic IR spectra (bottom) of the (2, 2, 1) cluster. Isomer A, B, and C are all relatively close in energy, with isomer A marginally lowest in energy. The main features involve OH stretching and bending modes (peaks in red), NH stretching and NH_2/ NH_3 bending modes (peaks in blue), and IO stretching modes (peaks in purple). Isomer A appears to be the experimentally present isomer, as it has a free OH stretching mode, a singular NH stretching mode, and a relative peak intensity pattern that is well replicated in the fingerprint region. The green dashed line in the isomer A structure represents a halogen bonding interaction, and the solid green lines highlighting a covalent bond in each of the structures represent likely intracluster covalent bond formation.

with an additional interaction. All of the higher energy isomers contain only one non-hydrogen bonding interaction. Similar to the (2, 1, 1) cluster, the (2, 2, 1) cluster exhibits almost equal bond lengths between what started as the iodine pentoxide and iodate constituents and the internal bond of what was the iodine pentoxide (bonds highlighted in green). These bond lengths are also slightly shorter than halogen bonds, but slightly longer than a typical I−O covalent bond, complicating the identification of the interaction taking place within the cluster. Once again isomer A has the fewest hydrogen bonds (six), whereas isomers B and C each have seven hydrogen bonds, and isomers D and E (SI Figure S11) have eight. This further reinforces the preferential importance of halogen bonding/non-hydrogen bonding interactions in stabilizing these clusters over that provided by hydrogen bonding. The (2, 2, 1) cluster shows the extension of the O−I−O backbone through both halogen bond formation and an additional stronger interaction, further emphasizing the role of these intermolecular forces in the growth of this type of cluster into larger, more atmospherically relevant sizes.

7. Halogen Bonding vs Covalent Bonding. Taking a closer look at the clusters that contain halogen bonds, we can see emerging themes for this type of cluster. Figure 7 depicts the structures of theses clusters excluding the (1, 0, 1) cluster as it does not involve halogen bonding and/or covalent-like bond formation. The (1, 2, 0) and (2, 2, 0) clusters differ by one ammonia, with the addition of ammonia resulting in deprotonation of one iodic acid. We see that difference reflected in the halogen bond interaction distance: in the (1, 2, 0) cluster, the hydrogen bond formed between the OH of one iodic acid and an oxygen of the other results in a more strained geometry that leads to a weaker halogen bond than in the (2, 2, 0) cluster. The addition of the second ammonium allows for a more optimal halogen bonding orientation to form, leading to a shorter halogen bond interaction and therefore a stronger halogen bond, as can be referenced in Table S1 (bond 2 versus bond 6). As discussed above, halogen bonding appears to be an important stabilizing interaction in these clusters. The experimentally determined structures of both the (1, 2, 0) and (2, 2, 0) clusters are capable of supporting one more hydrogen bond to an iodic acid OH group, but instead the formation of the halogen bond is favored.

In the larger clusters, we find hydrogen and halogen bonding in competition with covalent bond formation. At first glance, both larger clusters appear to contain an $I_3O_8^-$ molecule rather than distinct I_2O_5 and IO_3^- moieties. Examining the O−I−O backbone of the putative $I_3O_8^-$ in the (2, 1, 1) cluster structure, we see essentially identical bond lengths of 2.13 Å between bonds 10 and 11 (Figure 7 and Table S1), where we initially might have expected to find a halogen bond (bond highlighted in green, for example). These bonds are slightly longer than neighboring IO bonds 9 and 12, which also exhibit equal bond lengths of about 1.92 Å. Several observations of $I_3O_8^-$, for a range of applications, have been reported previously.

Metal iodates have been explored in nonlinear optics, such as NaI_3O_8, where the formation of the $I_3O_8^-$ ion was found to originate from the condensation of three iodate anions.[74] Studies on hydration mechanisms surrounding HIO_3 found that HI_3O_8 can form in a multistep dehydration process from iodic acid.[52,75] A quantum chemical study examining likely atmospheric interactions between I_2O_4, I_2O_5, HIO_2, and HIO_3

https://doi.org/10.1021/jacs.2c10841
J. Am. Chem. Soc. 2023, 145, 1165−1175

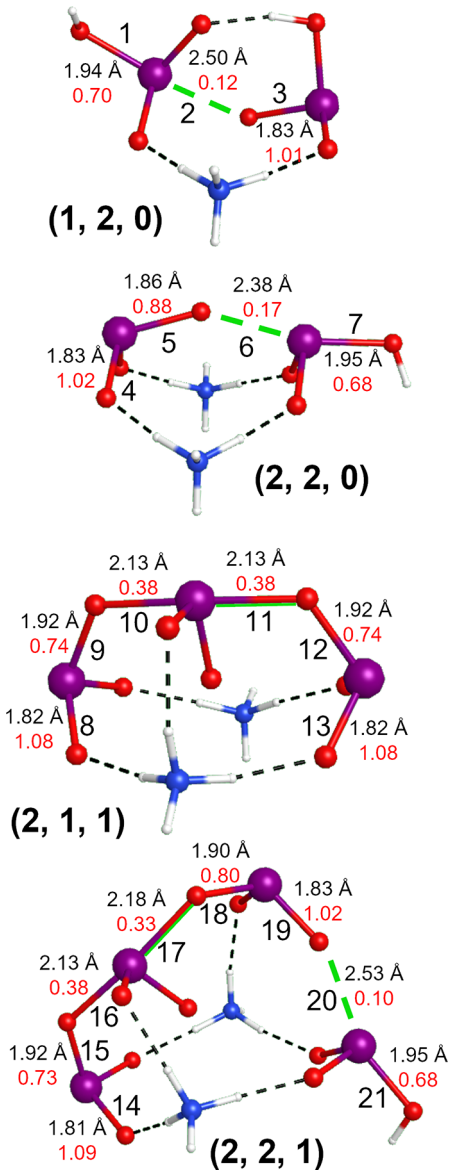

Figure 7. Experimentally identified structures of the (1, 2, 0), (2, 2, 0), (2, 1, 1), and (2, 2, 1) clusters that all contain halogen bonding and/or a new covalent-like bond. The green dashed lines in the cluster structures represent halogen bonding interactions. The (2, 1, 1) and (2, 2, 1) clusters both appear to exhibit covalent-like bond formation resulting in the presence of an intracluster $I_3O_8^-$ complex, depicted in the figure as a solid green line highlighting a single covalent bond. The O−I−O backbone bond lengths are displayed in black, with the respective Wiberg indices listed in red just below. All of the O−I−O backbone bonds are numbered as well, to aid in discussion.

with water have identified the prospect of the generation of an I_3O_8 complex as well.[54] Since the (2, 1, 1) cluster contains an iodate along with I_2O_5, which forms from the dehydration of two HIO_3 molecules, there is ample potential that an intracluster covalent $I_3O_8^-$ is forming.

We performed DFT calculations on both I_2O_5 and $I_3O_8^-$ molecules at the same level of theory as all of the clusters discussed above in order to compare bond lengths of the individual molecules to those of the clusters. Natural bond orbital calculations (NBO) were also performed on the four clusters displayed in Figure 7, as well as I_2O_5 and $I_3O_8^-$. The optimized $I_3O_8^-$ complex is found to have marginally longer bonds overall compared to I_2O_5. The central O in I_2O_5 is equally distanced from either I (2.01 Å), whereas the symmetric central bond lengths in $I_3O_8^-$ are 2.11 Å ($I_{central}$–$O_{central}$) and 1.95 Å ($O_{central}$–$I_{terminal}$). Terminal IO bond distances in both I_2O_5 and $I_3O_8^-$ are essentially equivalent to each other (1.80 and 1.81 Å, respectively). The optimized $I_3O_8^-$ structure exhibited comparable bond lengths to those of the suspected $I_3O_8^-$ complex within the (2, 1, 1) cluster, further supporting the hypothesis of intracluster covalent complex formation. The terminal and bridging IO bond lengths are all roughly 0.1 Å longer than those reported for the NaI_3O_8 crystal structure,[74] though it is unclear if this is related to the level of theory used here or differences between the cluster and crystal environments. The NBO calculations for the (2, 1, 1) cluster suggest that the interaction taking place at bond 11 is stronger than a halogen bond but slightly weaker interaction than a typical covalent IO bond. However, upon comparison to the NBO calculations of the $I_3O_8^-$ complex, we find very similar bond indices between the putative (2, 1, 1) $I_3O_8^-$ and the optimized $I_3O_8^-$, suggesting that the $I_3O_8^-$ present in these clusters is consistent with a free $I_3O_8^-$.

For the (2, 2, 1) cluster, we find both a halogen bond (bond 20 in Figure 7) and an apparent $I_3O_8^-$. The halogen bond, at about 2.53 Å, is significantly longer than the newly formed, presumable covalent bond (17, highlighted in green in Figure 7), which is approximately 2.18 Å. The $I_3O_8^-$ in this cluster features slightly asymmetric O−I−O backbone bonds, with bond 17 (green highlighted bond) slightly longer (2.18 Å) than bond 16 (2.13 Å). The neighboring IO bonds 15 and 18 in (2, 2, 1) are also found to be nonequivalent, unlike their counterparts in both the (2, 1, 1) cluster and $I_3O_8^-$. These slight differences in interaction distances are likely a result of a perturbation by the halogen bond (bond 20). The Wiberg indices of this cluster generated from the NBO calculations confirm that the longer bond (17) is slightly weaker than bond 16 as well as the equivalent bonds in the $I_3O_8^-$ molecule (Figure S13).

SUMMARY

In this study we investigated the compositions and structures of clusters involving ammonia, iodic acid, and iodine pentoxide via mass spectrometry, IR spectroscopy, and quantum chemistry. The lowest energy structures of some of the smallest clusters of this class were determined with high confidence using these techniques. This revealed the formation and expansion of the O−I−O backbone via both halogen bonding and likely also covalent bonding, resulting in the formation of $I_3O_8^-$ in the largest clusters investigated. Of the five clusters explored, this halogen/covalently bonded backbone appeared in the largest four clusters, suggesting this binding arrangement is likely important to the growth of these clusters into atmospherically relevant sizes. Halogen bonding appeared to outcompete hydrogen bonding in stabilizing these clusters, as all of the newly determined structures for the four largest clusters exhibited the fewest number of hydrogen bonds compared to all structures explored at that size and at least one halogen bond and/or new covalent-like bond. This further emphasizes the importance of these intermolecular forces in stabilizing and potentially accelerating the growth of these clusters. Ammonia also likely helps reduce the evaporation of these clusters through ionic interactions with iodic acid,

https://doi.org/10.1021/jacs.2c10841
J. Am. Chem. Soc. 2023, 145, 1165−1175

allowing these clusters to grow to larger sizes and may even catalyze the dehydration reaction between two iodic acid molecules to form I_2O_5. These results also suggest ammonia might improve growth of these clusters through hydrogen bonding interactions, by aligning incoming HIO_3 and I_2O_5 molecules into optimal positions such that halogen bonding and/or covalent bond formation can adequately take place, and may even facilitate the formation of the intracluster covalently bound $I_3O_8^-$ complex.

■ ASSOCIATED CONTENT

Supporting Information

The Supporting Information is available free of charge at https://pubs.acs.org/doi/10.1021/jacs.2c10841.

The Supporting Information contains justification for the level of theory used as well as additional experimental and calculated spectra comparisons, and coordinates for all of the computed clusters. (PDF)

■ AUTHOR INFORMATION

Corresponding Author

Christopher J. Johnson − *Department of Chemistry, Stony Brook University, Stony Brook, New York 11794, United States;* orcid.org/0000-0003-1859-5615; Email: chris.johnson@stonybrook.edu

Authors

Nicoline C. Frederiks − *Department of Chemistry, Stony Brook University, Stony Brook, New York 11794, United States;* orcid.org/0000-0002-1029-663X

Danika D. Heaney − *Department of Chemistry, Stony Brook University, Stony Brook, New York 11794, United States;* Present Address: Wellesley College, 106 Central St., Wellesley, MA 02481; orcid.org/0000-0001-5648-6394

John J. Kreinbihl − *Department of Chemistry, Stony Brook University, Stony Brook, New York 11794, United States;* orcid.org/0000-0003-4591-3375

Complete contact information is available at: https://pubs.acs.org/10.1021/jacs.2c10841

Notes

The authors declare no competing financial interest.

■ ACKNOWLEDGMENTS

This material is based upon work supported by the National Science Foundation under Grant No. CHE-1905172. DDH acknowledges support from the National Science Foundation Research Experiences for Undergraduates program under Grant No. CHE-2050541. Any opinions, findings, and conclusions or recommendations expressed in this material are those of the author(s) and do not necessarily reflect the views of the National Science Foundation.

■ REFERENCES

(1) Merikanto, J.; Spracklen, D.; Mann, G.; Pickering, S.; Carslaw, K. Impact of nucleation on global CCN. *Atmospheric Chemistry and Physics* **2009**, *9*, 8601−8616.

(2) Kulmala, M.; Riipinen, I.; Sipila, M.; Manninen, H. E.; Petaja, T.; Junninen, H.; Maso, M. D.; Mordas, G.; Mirme, A.; Vana, M.; et al. Toward direct measurement of atmospheric nucleation. *Science* **2007**, *318*, 89−92.

(3) Temelso, B.; Morrison, E. F.; Speer, D. L.; Cao, B. C.; Appiah-Padi, N.; Kim, G.; Shields, G. C. Effect of mixing ammonia and alkylamines on sulfate aerosol formation. *J. Phys. Chem. A* **2018**, *122*, 1612−1622.

(4) Jen, C. N.; McMurry, P. H.; Hanson, D. R. Stabilization of sulfuric acid dimers by ammonia, methylamine, dimethylamine, and trimethylamine. *Journal of Geophysical Research: Atmospheres* **2014**, *119*, 7502−7514.

(5) Lehtipalo, K.; Rondo, L.; Kontkanen, J.; Schobesberger, S.; Jokinen, T.; Sarnela, N.; Kürten, A.; Ehrhart, S.; Franchin, A.; Nieminen, T.; et al. The effect of acid−base clustering and ions on the growth of atmospheric nano-particles. *Nat. Commun.* **2016**, *7*, 1−9.

(6) Chen, M.; Titcombe, M.; Jiang, J.; Jen, C.; Kuang, C.; Fischer, M. L.; Eisele, F. L.; Siepmann, J. I.; Hanson, D. R.; Zhao, J.; et al. Acid−base chemical reaction model for nucleation rates in the polluted atmospheric boundary layer. *Proc. Natl. Acad. Sci. U. S. A.* **2012**, *109*, 18713−18718.

(7) Bianchi, F.; Praplan, A. P.; Sarnela, N.; Dommen, J.; Kurten, A.; Ortega, I. K.; Schobesberger, S.; Junninen, H.; Simon, M.; Trostl, J.; et al. Insight into acid−base nucleation experiments by comparison of the chemical composition of positive, negative, and neutral clusters. *Environ. Sci. Technol.* **2014**, *48*, 13675−13684.

(8) Smith, J. N.; Barsanti, K. C.; Friedli, H. R.; Ehn, M.; Kulmala, M.; Collins, D. R.; Scheckman, J. H.; Williams, B. J.; McMurry, P. H. Observations of aminium salts in atmospheric nanoparticles and possible climatic implications. *Proc. Natl. Acad. Sci. U. S. A.* **2010**, *107*, 6634−6639.

(9) Kulmala, M.; Petäjä, T.; Ehn, M.; Thornton, J.; Sipilä, M.; Worsnop, D.; Kerminen, V.-M. Chemistry of atmospheric nucleation: on the recent advances on precursor characterization and atmospheric cluster composition in connection with atmospheric new particle formation. *Annu. Rev. Phys. Chem.* **2014**, *65*, 21−37.

(10) Johnson, C. J.; Johnson, M. A. Vibrational spectra and fragmentation pathways of size-selected, D_2-tagged ammonium/methylammonium bisulfate clusters. *J. Phys. Chem. A* **2013**, *117*, 13265−13274.

(11) Waller, S. E.; Yang, Y.; Castracane, E.; Racow, E. E.; Kreinbihl, J. J.; Nickson, K. A.; Johnson, C. J. The interplay between hydrogen bonding and coulombic forces in determining the structure of sulfuric acid-amine clusters. *J. Phys. Chem. Lett.* **2018**, *9*, 1216−1222.

(12) Yang, Y.; Waller, S. E.; Kreinbihl, J. J.; Johnson, C. J. Direct link between structure and hydration in ammonium and aminium bisulfate clusters implicated in atmospheric new particle formation. *J. Phys. Chem. Lett.* **2018**, *9*, 5647−5652.

(13) Yang, Y.; Johnson, C. J. Hydration motifs of ammonium bisulfate clusters of relevance to atmospheric new particle formation. *Faraday Discuss.* **2019**, *217*, 47−66.

(14) Kreinbihl, J. J.; Frederiks, N. C.; Waller, S. E.; Yang, Y.; Johnson, C. J. Establishing the structural motifs present in small ammonium and aminium bisulfate clusters of relevance to atmospheric new particle formation. *J. Chem. Phys.* **2020**, *153*, 034307.

(15) Kreinbihl, J. J.; Frederiks, N. C.; Johnson, C. J. Hydration motifs of ammonium bisulfate clusters show complex temperature dependence. *J. Chem. Phys.* **2021**, *154*, 014304.

(16) Lee, S.-H.; Gordon, H.; Yu, H.; Lehtipalo, K.; Haley, R.; Li, Y.; Zhang, R. New particle formation in the atmosphere: From molecular clusters to global climate. *Journal of Geophysical Research: Atmospheres* **2019**, *124*, 7098−7146.

(17) O'Dowd, C.; McFiggans, G.; Creasey, D. J.; Pirjola, L.; Hoell, C.; Smith, M. H.; Allan, B. J.; Plane, J. M.; Heard, D. E.; Lee, J. D.; et al. On the photochemical production of new particles in the coastal boundary layer. *Geophys. Res. Lett.* **1999**, *26*, 1707−1710.

(18) O'Dowd, C. D.; Hämeri, K.; Mäkelä, J. M.; Pirjola, L.; Kulmala, M.; Jennings, S. G.; Berresheim, H.; Hansson, H.-C.; De Leeuw, G.; Kunz, G. J., et al.A dedicated study of New Particle Formation and Fate in the Coastal Environment (PARFORCE): Overview of objectives and achievements. *Journal of Geophysical Research: Atmospheres*2002, *107*, PAR−1.

(19) Hoffmann, T.; O'Dowd, C. D.; Seinfeld, J. H. Iodine oxide homogeneous nucleation: An explanation for coastal new particle production. *Geophys. Res. Lett.* **2001**, *28*, 1949−1952.
(20) Laturnus, F. Volatile halocarbons released from Arctic macroalgae. *Marine Chemistry* **1996**, *55*, 359−366.
(21) Carpenter, L.; Sturges, W.; Penkett, S.; Liss, P.; Alicke, B.; Hebestreit, K.; Platt, U. Short-lived alkyl iodides and bromides at Mace Head, Ireland: Links to biogenic sources and halogen oxide production. *Journal of Geophysical Research: Atmospheres* **1999**, *104*, 1679−1689.
(22) Alicke, B.; Hebestreit, K.; Stutz, J.; Platt, U. Iodine oxide in the marine boundary layer. *Nature* **1999**, *397*, 572−573.
(23) McFiggans, G.; Coe, H.; Burgess, R.; Allan, J.; Cubison, M.; Alfarra, M. R.; Saunders, R.; Saiz-Lopez, A.; Plane, J.; Wevill, D.; et al. Direct evidence for coastal iodine particles from Laminaria macroalgae−linkage to emissions of molecular iodine. *Atmospheric Chemistry and Physics* **2004**, *4*, 701−713.
(24) Saiz-Lopez, A.; Plane, J.; McFiggans, G.; Williams, P.; Ball, S.; Bitter, M.; Jones, R.; Hongwei, C.; Hoffmann, T. Modelling molecular iodine emissions in a coastal marine environment: the link to new particle formation. *Atmospheric Chemistry and Physics* **2006**, *6*, 883−895.
(25) Palmer, C. J.; Anders, T. L.; Carpenter, L. J.; Küpper, F. C.; McFiggans, G. B. Iodine and halocarbon response of Laminaria digitata to oxidative stress and links to atmospheric new particle production. *Environmental Chemistry* **2005**, *2*, 282−290.
(26) Leigh, R.; Ball, S.; Whitehead, J.; Leblanc, C.; Shillings, A.; Mahajan, A.; Oetjen, H.; Lee, J.; Jones, C.; Dorsey, J.; et al. Measurements and modelling of molecular iodine emissions, transport and photodestruction in the coastal region around Roscoff. *Atmospheric Chemistry and Physics* **2010**, *10*, 11823−11838.
(27) Hill, V. L.; Manley, S. L. Release of reactive bromine and iodine from diatoms and its possible role in halogen transfer in polar and tropical oceans. *Limnology and Oceanography* **2009**, *54*, 812−822.
(28) Saiz-Lopez, A.; Blaszczak-Boxe, C. S.; Carpenter, L. A mechanism for biologically induced iodine emissions from sea ice. *Atmospheric Chemistry and Physics* **2015**, *15*, 9731−9746.
(29) Atkinson, H. M.; Huang, R.-J.; Chance, R.; Roscoe, H. K.; Hughes, C.; Davison, B.; Schönhardt, A.; Mahajan, A. S.; Saiz-Lopez, A.; Hoffmann.; et al. Iodine emissions from the sea ice of the Weddell Sea. *Atmospheric Chemistry and Physics* **2012**, *12*, 11229−11244.
(30) Jimenez, J. L.; Bahreini, R.; Cocker, D. R., III; Zhuang, H.; Varutbangkul, V.; Flagan, R. C.; Seinfeld, J. H.; O'Dowd, C. D.; Hoffmann, T. New particle formation from photooxidation of diiodomethane (CH_2I_2). *Journal of Geophysical Research: Atmospheres* **2003**, *108*, 4318.
(31) Mäkelä, J.; Hoffmann, T.; Holzke, C.; Väkevä, M.; Suni, T.; Mattila, T.; Aalto, P.; Tapper, U.; Kauppinen, E. I.; O'Dowd, C.Biogenic iodine emissions and identification of end-products in coastal ultrafine particles during nucleation bursts. *Journal of Geophysical Research: Atmospheres*2002, *107*, PAR−14.
(32) O'Dowd, C. D.; Jimenez, J. L.; Bahreini, R.; Flagan, R. C.; Seinfeld, J. H.; Hämeri, K.; Pirjola, L.; Kulmala, M.; Jennings, S. G.; Hoffmann, T. Marine aerosol formation from biogenic iodine emissions. *Nature* **2002**, *417*, 632−636.
(33) Baccarini, A.; Karlsson, L.; Dommen, J.; Duplessis, P.; Vüllers, J.; Brooks, I. M.; Saiz-Lopez, A.; Salter, M.; Tjernström, M.; Baltensperger, U.; et al. Frequent new particle formation over the high Arctic pack ice by enhanced iodine emissions. *Nat. Commun.* **2020**, *11*, 1−11.
(34) Sipilä, M.; Sarnela, N.; Jokinen, T.; Henschel, H.; Junninen, H.; Kontkanen, J.; Richters, S.; Kangasluoma, J.; Franchin, A.; Peräkylä, O.; et al. Molecular-scale evidence of aerosol particle formation via sequential addition of HIO_3. *Nature* **2016**, *537*, 532−534.
(35) Saiz-Lopez, A.; Boxe, C. A mechanism for biologically-induced iodine emissions from sea-ice. *Atmospheric Chemistry and Physics Discussions* **2008**, *8*, 2953−2976.
(36) Gómez Martín, J. C.; Lewis, T. R.; Blitz, M. A.; Plane, J.; Kumar, M.; Francisco, J. S.; Saiz-Lopez, A. A gas-to-particle conversion mechanism helps to explain atmospheric particle formation through clustering of iodine oxides. *Nat. Commun.* **2020**, *11*, 1−14.
(37) Allan, B. J.; McFiggans, G.; Plane, J. M.; Coe, H. Observations of iodine monoxide in the remote marine boundary layer. *Journal of Geophysical Research: Atmospheres* **2000**, *105*, 14363−14369.
(38) Saiz-Lopez, A.; Plane, J. M. Novel iodine chemistry in the marine boundary layer. *Geophys. Res. Lett.* **2004**, *31*, L04112.
(39) Saiz-Lopez, A.; Plane, J. M.; Baker, A. R.; Carpenter, L. J.; von Glasow, R.; Gómez Martín, J. C.; McFiggans, G.; Saunders, R. W. Atmospheric chemistry of iodine. *Chem. Rev.* **2012**, *112*, 1773−1804.
(40) Moore, R.; Webb, M.; Tokarczyk, R.; Wever, R. Bromoperoxidase and iodoperoxidase enzymes and production of halogenated methanes in marine diatom cultures. *Journal of Geophysical Research: Oceans* **1996**, *101*, 20899−20908.
(41) O'Dowd, C. D.; Hämeri, K.; Mäkelä, J.; Väkeva, M.; Aalto, P.; de Leeuw, G.; Kunz, G. J.; Becker, E.; Hansson, H.-C.; Allen, A. G., et al.Coastal new particle formation: Environmental conditions and aerosol physicochemical characteristics during nucleation bursts. *Journal of Geophysical Research: Atmospheres*2002, *107*, PAR−12.
(42) Huang, R.; Seitz, K.; Neary, T.; O'Dowd, C.; Platt, U.; Hoffmann, T. Observations of high concentrations of I_2 and IO in coastal air supporting iodine−oxide driven coastal new particle formation. *Geophys. Res. Lett.* **2010**, *37*, L03803.
(43) Yu, H.; Ren, L.; Huang, X.; Xie, M.; He, J.; Xiao, H. Iodine speciation and size distribution in ambient aerosols at a coastal new particle formation hotspot in China. *Atmospheric Chemistry and Physics* **2019**, *19*, 4025−4039.
(44) Prados-Roman, C.; Cuevas, C. A.; Fernandez, R. P.; Kinnison, D. E.; Lamarque, J. F.; Saiz-Lopez, A. A negative feedback between anthropogenic ozone pollution and enhanced ocean emissions of iodine. *Atmospheric Chemistry and Physics* **2015**, *15*, 2215−2224.
(45) Martino, M.; Mills, G. P.; Woeltjen, J.; Liss, P. S. A new source of volatile organoiodine compounds in surface seawater. *Geophys. Res. Lett.* **2009**, *36*, L01609.
(46) Garland, J.; Curtis, H. Emission of iodine from the sea surface in the presence of ozone. *Journal of Geophysical Research: Oceans* **1981**, *86*, 3183−3186.
(47) Carpenter, L. J.; MacDonald, S. M.; Shaw, M. D.; Kumar, R.; Saunders, R. W.; Parthipan, R.; Wilson, J.; Plane, J. Atmospheric iodine levels influenced by sea surface emissions of inorganic iodine. *Nature Geoscience* **2013**, *6*, 108−111.
(48) He, X.-C.; Tham, Y. J.; Dada, L.; Wang, M.; Finkenzeller, H.; Stolzenburg, D.; Iyer, S.; Simon, M.; Kürten, A.; Shen, J.; et al. Role of iodine oxoacids in atmospheric aerosol nucleation. *Science* **2021**, *371*, 589−595.
(49) Gómez Martín, J. C.; Lewis, T. R.; James, A. D.; Saiz-Lopez, A.; Plane, J. M. Insights into the Chemistry of Iodine New Particle Formation: The Role of Iodine Oxides and the Source of Iodic Acid. *J. Am. Chem. Soc.* **2022**, *144*, 9240−9253.
(50) Xia, D.; Chen, J.; Yu, H.; Xie, H.-b.; Wang, Y.; Wang, Z.; Xu, T.; Allen, D. T. Formation Mechanisms of Iodine−Ammonia Clusters in Polluted Coastal Areas Unveiled by Thermodynamics and Kinetic Simulations. *Environ. Sci. Technol.* **2020**, *54*, 9235−9242.
(51) Rong, H.; Liu, J.; Zhang, Y.; Du, L.; Zhang, X.; Li, Z. Nucleation mechanisms of iodic acid in clean and polluted coastal regions. *Chemosphere* **2020**, *253*, 126743.
(52) Smith, D. K.; Pantoya, M. L.; Parkey, J. S.; Kesmez, M. The water−iodine oxide system: a revised mechanism for hydration and dehydration. *RSC Adv.* **2017**, *7*, 10183−10191.
(53) Khanniche, S.; Louis, F.; Cantrel, L.; Černušák, I. Computational study of the $I_2O_5 + H_2O = 2HOIO_2$ gas-phase reaction. *Chem. Phys. Lett.* **2016**, *662*, 114−119.
(54) Kumar, M.; Saiz-Lopez, A.; Francisco, J. S. Single-molecule catalysis revealed: elucidating the mechanistic framework for the formation and growth of atmospheric iodine oxide aerosols in gas-phase and aqueous surface environments. *J. Am. Chem. Soc.* **2018**, *140*, 14704−14716.

https://doi.org/10.1021/jacs.2c10841
J. Am. Chem. Soc. 2023, 145, 1165−1175

(55) Ahonen, L.; Li, C.; Kubecka, J.; Iyer, S.; Vehkamaki, H.; Petaja, T.; Kulmala, M.; Hogan, C. J., Jr Ion mobility-mass spectrometry of iodine pentoxide−iodic acid hybrid cluster Anions in dry and humidified atmospheres. *J. Phys. Chem. Lett.* **2019**, *10*, 1935−1941.
(56) Pechtl, S.; Lovejoy, E.; Burkholder, J.; Von Glasow, R. Modeling the possible role of iodine oxides in atmospheric new particle formation. *Atmospheric Chemistry and Physics* **2006**, *6*, 505−523.
(57) Daly, S. M.; O'Connor, D. J.; Healy, D. A.; Hellebust, S.; Arndt, J.; McGillicuddy, E. J.; Feeney, P.; Quirke, M.; Wenger, J. C.; Sodeau, J. R. Investigation of coastal sea-fog formation using the WIBS (wideband integrated bioaerosol sensor) technique. *Atmospheric Chemistry and Physics* **2019**, *19*, 5737−5751.
(58) Allan, J.; Williams, P. I.; Najera, J.; Whitehead, J.; Flynn, M.; Taylor, J.; Liu, D.; Darbyshire, E.; Carpenter, L.; Chance, R.; et al. Iodine observed in new particle formation events in the Arctic atmosphere during ACCACIA. *Atmospheric Chemistry and Physics* **2015**, *15*, 5599−5609.
(59) Ning, A.; Liu, L.; Ji, L.; Zhang, X. Molecular-level evidence for marine aerosol nucleation of iodic acid and methanesulfonic acid. *Atmospheric Chemistry and Physics Discussions* **2021**, *2021*, 1−20.
(60) Gálvez, O.; Martín, J. G.; Gómez, P. C.; Saiz-Lopez, A.; Pacios, L. F. A theoretical study on the formation of iodine oxide aggregates and monohydrates. *Phys. Chem. Chem. Phys.* **2013**, *15*, 15572−15583.
(61) He, X.-C.; Iyer, S.; Sipilä, M.; Ylisirnïo, A.; Peltola, M.; Kontkanen, J.; Baalbaki, R.; Simon, M.; Kürten, A.; Tham, Y. J.; et al. Determination of the collision rate coefficient between charged iodic acid clusters and iodic acid using the appearance time method. *Aerosol Sci. Technol.* **2021**, *55*, 231−242.
(62) Burkholder, J.; Curtius, J.; Ravishankara, A.; Lovejoy, E. Laboratory studies of the homogeneous nucleation of iodine oxides. *Atmospheric Chemistry and Physics* **2004**, *4*, 19−34.
(63) Saunders, R.; Kumar, R.; Martín, J. G.; Mahajan, A.; Murray, B.; Plane, J. Studies of the formation and growth of aerosol from molecular iodine precursor. *Zeitschrift für Physikalische Chemie* **2010**, *224*, 1095−1117.
(64) Kumar, R.; Saunders, R.; Mahajan, A.; Plane, J.; Murray, B. Physical properties of iodate solutions and the deliquescence of crystalline I_2O_5 and HIO_3. *Atmospheric Chemistry and Physics* **2010**, *10*, 12251−12260.
(65) Waller, S. E.; Yang, Y.; Castracane, E.; Kreinbihl, J. J.; Nickson, K. A.; Johnson, C. J. Electrospray Ionization−Based Synthesis and Validation of Amine-Sulfuric Acid Clusters of Relevance to Atmospheric New Particle Formation. *Journal of The American Society for Mass Spectrometry* **2019**, *30*, 2267−2277.
(66) Wolk, A. B.; Leavitt, C. M.; Garand, E.; Johnson, M. A. Cryogenic ion chemistry and spectroscopy. *Acc. Chem. Res.* **2014**, *47*, 202−210.
(67) Frisch, M. J.et al.*Gaussian 16*, Revision A.03; Gaussian Inc.: 2016.
(68) Weinhold, F.*Discovering chemistry with natural bond orbitals*; John Wiley & Sons: 2012.
(69) DeBlase, A. F.; Bloom, S.; Lectka, T.; Jordan, K. D.; McCoy, A. B.; Johnson, M. A. Origin of the diffuse vibrational signature of a cyclic intramolecular proton bond: anharmonic analysis of protonated 1, 8-disubstituted naphthalene ions. *J. Chem. Phys.* **2013**, *139*, 024301.
(70) Johnson, C. J.; Dzugan, L. C.; Wolk, A. B.; Leavitt, C. M.; Fournier, J. A.; McCoy, A. B.; Johnson, M. A. Microhydration of Contact Ion Pairs in M^{2+} $OH^-(H_2O)_{n=1-5}$ (M = Mg, Ca) Clusters: Spectral Manifestations of a Mobile Proton Defect in the First Hydration Shell. *J. Phys. Chem. A* **2014**, *118*, 7590−7597.
(71) Headrick, J. M.; Diken, E. G.; Walters, R. S.; Hammer, N. I.; Christie, R. A.; Cui, J.; Myshakin, E. M.; Duncan, M. A.; Johnson, M. A.; Jordan, K. D. Spectral signatures of hydrated proton vibrations in water clusters. *Science* **2005**, *308*, 1765−1769.
(72) Roscioli, J.; McCunn, L.; Johnson, M. Quantum structure of the intermolecular proton bond. *Science* **2007**, *316*, 249−254.
(73) Johnson, C. J.; Wolk, A. B.; Fournier, J. A.; Sullivan, E. N.; Weddle, G. H.; Johnson, M. A. Communication: He-tagged vibrational spectra of the $SarGlyH^+$ and $H^+(H_2O)_{2,3}$ ions: Quantifying tag effects in cryogenic ion vibrational predissociation (CIVP) spectroscopy. *J. Chem. Phys.* **2014**, *140*, 221101.
(74) Phanon, D.; Gautier-Luneau, I. Promising material for infrared nonlinear optics: NaI_3O_8 salt containing an octaoxotriiodate (V) anion formed from condensation of $[IO_3]^-$ ions. *Angew. Chem., Int. Ed.* **2007**, *46*, 8488−8491.
(75) Selte, K.; Kjekshus, A. Iodine Oxides. *Acta Chemica Scandanvica* **1968**, *22*, 3309−3320.

https://doi.org/10.1021/jacs.2c10841
J. Am. Chem. Soc. 2023, 145, 1165−1175